

Domain Walls in Normal and Superconducting States of Iron Pnictides

Huaxiang Huang,^{1,2} Degang Zhang,¹ Tao Zhou,^{3,1} and C. S. Ting¹

¹*Texas Center for Superconductivity and Department of Physics,
University of Houston, Houston, Texas 77204, USA*

²*Department of Physics, Shanghai University, Shanghai 200444, China*

³*College of Science, Nanjing University of Aeronautics and Astronautics, Nanjing 210016, China*

The electronic and magnetic structures in the normal and superconducting states of iron pnictides are investigated by solving self-consistently the Bogoliubov-de Gennes equation. It is shown that strong electron correlations can induce domain walls, which separate regions with different spin density wave orders. At zero or low electron doping, 90° domain walls are formed while anti-phase domain walls are produced at higher electron doping. On the domain walls, larger electron densities are always present. The results agree qualitatively with recent observations of scanning tunneling microscopy and superconducting quantum interference device microscopy.

PACS numbers: 74.70.Xa, 75.60.Ch, 74.25.-q, 74.81.-g

The discovery of a new family of layered superconductors, i.e., the FeAs-based superconductors, could offer a new avenue to explore the mechanism of high temperature superconductivity [1-5]. Similar to the cuprates, the parent compounds of the FeAs-based superconductors also possess the antiferromagnetic ground state [4,5]. With increasing electron or hole doping, antiferromagnetic order is suppressed and superconductivity appears in both the cuprates and the iron pnictides. However, different from the cuprates, due to the strong nesting effect between the hole Fermi surfaces around the Γ point and the electron Fermi surfaces around the M point, superconductivity and the spin density wave (SDW) orders can coexist in the electron-doped FeAs-based superconductors [6,7]. Because each unit cell of the FeAs-based superconductors contains two inequivalent Fe ions, different arrays of magnetic moments on Fe ions in both normal and superconducting states could lead to diverse magnetic structures and uncommon electronic properties [8,9].

Recently, in scanning tunneling microscopy (STM) experiments twin boundaries were observed in the normal state of $\text{Ca}(\text{Fe}_{1-x}\text{Co}_x)_2\text{As}_2$ [10]. Across these twin boundaries, the a (b) axis of the crystal rotates through 90°. This means that the modulation direction of SDW is rotated by 90°. In other words, 90° domain walls are formed at the twin boundaries. In Ref. [11], superconducting quantum interference device microscopy (SQIDM) revealed that in the superconducting state of underdoped $\text{Ba}(\text{Fe}_{1-x}\text{Co}_x)_2\text{As}_2$ with $x < 0.07$, the diamagnetic susceptibility is increased and the superfluid density is enhanced on the twin boundaries or 90° domain walls. In another STM experiment [12], Li *et al.* also observed a 90° anti-phase domain wall in the parent compounds of iron pnictides, on which the local density of states (LDOS) is much higher than that in the interior of magnetic domains. Therefore, domain walls exist universally in underdoped FeAs-based superconductors and affect strongly the electronic properties in the normal and

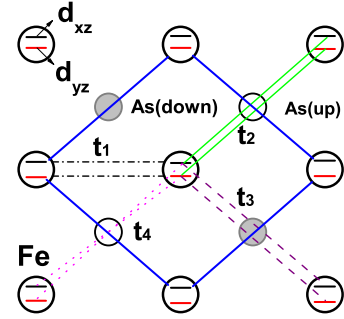


FIG. 1: (Color online) Schematic of the tight-binding model H_0 in Ref. [13]. t_1 is the nearest neighbor hopping between the same orbitals d_{xz} or d_{yz} on Fe ions, t_2 and t_3 are the next-nearest neighbor hoppings between the same orbitals mediated by the up and down As ions, respectively, and t_4 is the next nearest neighboring hopping between the different orbitals.

superconducting states.

In this work, we study the complex electronic and magnetic structures in the underdoped FeAs-based superconductors by solving self-consistently the Bogoliubov-de Gennes (BdG) equation. We start from the model Hamiltonian $H = H_0 + H_{SC} + H_{int}$. Here H_0 is the two-orbital four-band tight-binding model proposed in Ref. [13], which describes correctly the characteristics of the energy band structure for the FeAs-based superconductors [14-19]. The hopping parameters t_1 - t_4 in H_0 are depicted in Fig. 1.

The pairing Hamiltonian

$$H_{SC} = \sum_{\mathbf{i}\mu\mathbf{j}\nu} (\Delta_{\mathbf{i}\mu\mathbf{j}\nu} c_{\mathbf{i}\mu\uparrow}^\dagger c_{\mathbf{j}\nu\downarrow}^\dagger + \text{h.c.}), \quad (1)$$

where $\Delta_{\mathbf{i}\mu\mathbf{j}\nu}$ is the pairing between the orbital μ (d_{xz} or d_{yz}) on the site \mathbf{i} and the orbital ν (d_{xz} or d_{yz}) on the site \mathbf{j} , and $c_{\mathbf{i}\mu\sigma}^\dagger$ is the creation operator of an electron with

spin σ at the orbital μ on the site \mathbf{i} .

The interaction Hamiltonian H_{int} considered here only includes on-site Coulomb interaction U and Hund coupling J_H . After taking the mean field treatment, H_{int} can be expressed as [20]

$$H_{int} = U \sum_{\mathbf{i}, \mu, \sigma \neq \bar{\sigma}} \langle n_{\mathbf{i}\mu\bar{\sigma}} \rangle n_{\mathbf{i}\mu\sigma} + (U - 3J_H) \sum_{\mathbf{i}, \mu \neq \nu, \sigma} \langle n_{\mathbf{i}\mu\sigma} \rangle n_{\mathbf{i}\nu\sigma} \\ + (U - 2J_H) \sum_{\mathbf{i}, \mu \neq \nu, \sigma \neq \bar{\sigma}} \langle n_{\mathbf{i}\mu\bar{\sigma}} \rangle n_{\mathbf{i}\nu\sigma}, \quad (2)$$

where $n_{\mathbf{i}\mu\sigma} = c_{\mathbf{i}\mu\sigma}^\dagger c_{\mathbf{i}\mu\sigma}$.

We note that based on the model Hamiltonian H , the obtained LDOS[13,20], phase diagram [20], and spin susceptibility at different doping and temperature [21] for electron doped FeAs-based superconductors, and Andreev bound states at negative energy inside the vortex core [22] for hole doped FeAs-based superconductors are all consistent with the STM [23-26], nuclear magnetic resonance [6,7], and neutron scattering experiments [27-30].

The eigenvalues and eigenfunctions of H can be obtained by solving self-consistently the BdG equation, i.e.

$$\sum_{\mathbf{j}, \nu} \begin{pmatrix} H_{\mathbf{i}\mu\mathbf{j}\nu\sigma} & \Delta_{\mathbf{i}\mu\mathbf{j}\nu} \\ \Delta_{\mathbf{i}\mu\mathbf{j}\nu}^* & -H_{\mathbf{i}\mu\mathbf{j}\nu\bar{\sigma}} \end{pmatrix} \begin{pmatrix} u_{\mathbf{j}\nu\sigma}^n \\ v_{\mathbf{j}\nu\bar{\sigma}}^n \end{pmatrix} = E_n \begin{pmatrix} u_{\mathbf{i}\mu\sigma}^n \\ v_{\mathbf{i}\mu\bar{\sigma}}^n \end{pmatrix}, \quad (3)$$

where $H_{\mathbf{i}\mu\mathbf{j}\nu\sigma}$ is the matrix element of H with spin σ between the orbital μ on the site \mathbf{i} and the orbital ν on the site \mathbf{j} . The superconducting pairing $\Delta_{\mathbf{i}\mu\mathbf{j}\nu} \equiv \frac{1}{2} \langle c_{\mathbf{i}\mu\uparrow} c_{\mathbf{j}\nu\downarrow} - c_{\mathbf{i}\mu\downarrow} c_{\mathbf{j}\nu\uparrow} \rangle$ in real space is associated with the eigenvalues E_n and the eigenfunctions $(u_{\mathbf{i}\mu\sigma}^n, v_{\mathbf{i}\mu\bar{\sigma}}^n)$, and has the form

$$\Delta_{\mathbf{i}\mu\mathbf{j}\nu} = \frac{V_{\mathbf{i}\mu\mathbf{j}\nu}}{4} \sum_n (u_{\mathbf{i}\mu\uparrow}^n v_{\mathbf{j}\nu\downarrow}^{n*} + u_{\mathbf{j}\nu\uparrow}^n v_{\mathbf{i}\mu\downarrow}^{n*}) \tanh\left(\frac{E_n}{2k_B T}\right) \quad (4)$$

at temperature T . Here, k_B is the Boltzmann's constant, and $V_{\mathbf{i}\mu\mathbf{j}\nu}$ is the pairing potential between the orbitals on the sites \mathbf{i} and \mathbf{j} . The corresponding local electron density reads

$$n_{\mathbf{i}} = \sum_{n, \mu} \{ |u_{\mathbf{i}\mu\uparrow}^n|^2 f(E_n) + |v_{\mathbf{i}\mu\downarrow}^n|^2 [1 - f(E_n)] \}, \quad (5)$$

where $f(E_n)$ is the Fermi function, and the local magnetic moment $m_{\mathbf{i}} = \frac{1}{2} \sum_{\mu} (\langle n_{\mathbf{i}\mu\uparrow} \rangle - \langle n_{\mathbf{i}\mu\downarrow} \rangle)$.

In order to interpret the complex domain wall structures seen by STM experiments on the iron pnictides, we investigate the strong Coulomb correlation on Fe sites. In our calculations, we have employed the hopping parameters in Ref. [13], i.e. $t_1 = 1$, $t_2 = 0.4$, $t_3 = -2.0$, and $t_4 = 0.04$, and have chosen $U = 4.8$, $J_H = 1.3$, and $V_{\mathbf{i}\mu\mathbf{j}\nu} = 1.1$ for $\mu = \nu$ and $|\mathbf{i} - \mathbf{j}| = \sqrt{2}$, and 0 for all other cases. Note that only the electron pairings between the

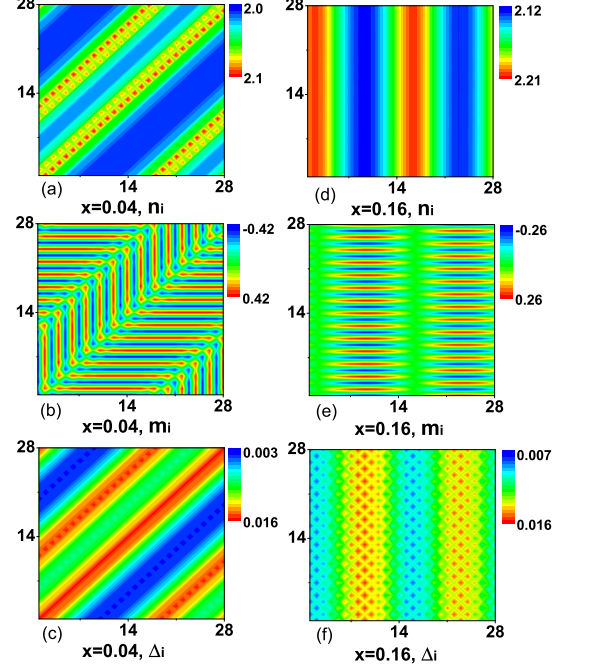


FIG. 2: (Color online) The images of electron density n_i , magnetic order m_i , and superconducting order Δ_i at electron dopings $x = 0.04$ and 0.16 .

same orbitals on the next nearest neighboring Fe sites are considered. Such a choice of the pairing potential leads the superconducting order parameter to be s_{\pm} -wave type.

In Fig. 2, we present the zero temperature images of electron density n_i , magnetic order m_i , and superconducting order $\Delta_i \equiv \frac{1}{8} \sum_{\mathbf{j}, \mu} \Delta_{\mathbf{i}\mu\mathbf{j}\mu}$ at electron dopings $x = 0.04$ and 0.16 on a 28×28 lattice with period boundary condition. From Fig. 2 (b) and (e), we can see that there exist obviously magnetic domain structures. Across the domain walls, the modulation direction of magnetic order rotates through 90° at $x = 0.04$ while the phase of magnetic order changes sign at $x = 0.16$. So the anti-phase domain walls, predicted previously in Ref. [8], are realized in the higher electron doped case. We observe that on both 90° domain walls and anti-phase domain walls, there are always higher electron densities n_i , as shown in Fig. 2 (a) and (d). Therefore, it is expected that superfluid density is enhanced on these domain walls, which coincides with the observations of SQIDM experiments [11]. However, the superconducting order parameter Δ_i has a larger magnitude on 90° domain walls, but has a smaller magnitude on anti-phase domain walls (see. Fig.2 (c) and (f)).

In order to see clearly the variations of n_i , m_i , and Δ_i with distance from the domain walls, in Fig. 3, we give their values on the line $y = 14$. Fig. 3(a) and

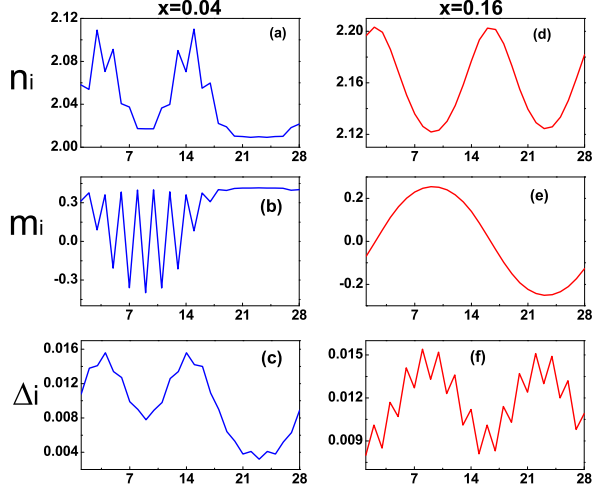


FIG. 3: (Color online) Electron density n_i , magnetic order m_i , and superconducting order Δ_i on the line $y = 14$ at electron dopings $x = 0.04$ and 0.16 .

(d) show that more electrons are accumulated near all the domain walls. On 90° domain walls at $x = 0.04$ in Fig. 3(b) and (c), both m_i and Δ_i have their maximum values. Oppositely, on anti-phase domain walls at $x = 0.16$ in Fig. 3(e) and (f), m_i almost vanishes, and Δ_i has the minimum values. Therefore, except for the electron density, the magnetic and superconducting properties on the two kinds of domain walls are very different.

We would like to mention that when $x < \sim 0.02$, n_i and m_i have similar patterns with those at $x = 0.04$, except $\Delta_i = 0$. Therefore, the 90° domain wall structure also exists in the normal state of the FeAs-based superconductors, and is consistent with the observations of STM experiments [10]. However, we do not get the solution of complex 90° anti-phase domain wall seen in the parent compounds [12], which cannot be formed under the period boundary condition.

Our calculations also show that with increasing electron doping, the magnetic order m_i is gradually suppressed and finally vanishes at $x \sim 0.2$, which is larger than the experimental value. The main difference between the theoretical results and experimental data could be due to the fact that a strong Coulomb interaction U leads to renormalization of the hole Fermi surfaces around the Γ point and the electron Fermi surfaces around the M point in the FeAs-based superconductors, which enhances the nesting effect between the hole Fermi surfaces and the electron Fermi surfaces. However, by adjusting suitably the hopping parameters t_2 and t_3 in H_0 , which determine the sizes and shapes of the Fermi surfaces, the nesting effect could be diminished and the experimental value can be obtained. When

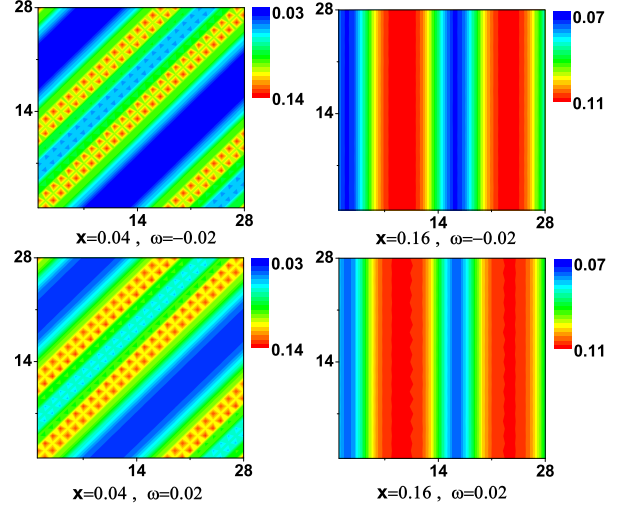


FIG. 4: (Color online) The images of LDOS $\rho_i(\omega)$ with electron dopings $x = 0.04$ and 0.16 at energies $\omega = \pm 0.02$.

$x < \sim 0.08$, the 90° domain walls always exist while the anti-phase magnetic domains show up at $x > \sim 0.15$. When $\sim 0.08 < x < \sim 0.15$, SDW and superconductivity uniformly coexist. We also note that the solution of anti-phase domain wall structure is a metastable state in the above range, which has a slightly higher energy than the ground state.

Now we calculate the LDOS on and near the domain walls in order to compare with the STM experiments. The expression of LDOS at energy ω on the site \mathbf{i} is

$$\rho_i(\omega) = \frac{1}{N} \sum_{n\mu\mathbf{k}} \{ |u_{i\mu\uparrow\mathbf{k}}^n|^2 \delta(E_{n\mathbf{k}} - \omega) + |v_{i\mu\downarrow\mathbf{k}}^n|^2 \delta(E_{n\mathbf{k}} + \omega) \}, \quad (6)$$

where N is the number of wave vectors \mathbf{k} , $(u_{i\mu\uparrow\mathbf{k}}^n, v_{i\mu\downarrow\mathbf{k}}^n)$ and $E_{n\mathbf{k}}$ are the eigenfunctions and eigenvalues of the Fourier transformed BdG equation, respectively. In calculating $\rho_i(\omega)$, we have taken the delta function $\delta(x) = \Gamma/\pi(x^2 + \Gamma^2)$ with quasiparticle damping $\Gamma = 0.005$, and a 30×30 supercell is used.

Fig. 4 shows the LDOS images on a 28×28 lattice at different energies and electron dopings. It is obvious that when $\omega = \pm 0.02$, $\rho_i(\omega)$ has the maximum value on the 90° domain walls at $x = 0.04$, but has the minimum value on the anti-phase domain walls at $x = 0.16$. Here we also omit the LDOS image with $x = 0.0$, which is similar to that of $x = 0.04$.

However, the LDOS images change with energy ω . In Fig. 5, we give the energy dependence of the LDOS $\rho_i(\omega)$ at the sites on and near domain walls with different electron dopings. In both $x = 0.0$ and 0.04 , obvi-

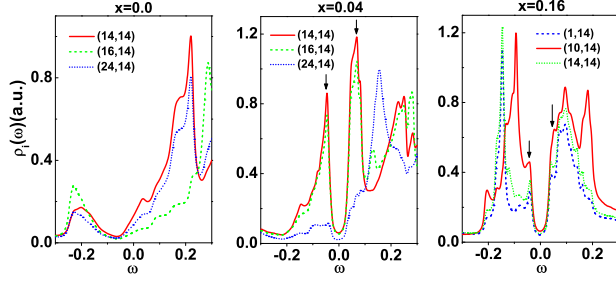


FIG. 5: (Color online) Energy dependence of LDOS $\rho_i(\omega)$ with electron dopings $x = 0.0, 0.04$, and 0.16 at the sites on and near domain walls. The arrows point to the coherence peaks with maximum superconducting order parameter Δ_i in the panels of $x = 0.04$ and 0.16

ously, $\rho_i(\omega)$ at (14, 14) on the 90° domain wall is always larger than that on the other sites when $\omega \in (-0.18, 0.1)$. In contrast, $\rho_i(\omega)$ at (1, 14) on the anti-phase domain wall is always smaller than that on the other sites when $\omega > -0.13$. We note that when $\omega \in (-0.2, 0.2)$, the curves of $\rho_i(\omega)$ with $x = 0.0$ resemble those measured by the STM experiments in the parent compounds [25]. The coherence peak at positive energy is higher at both $x = 0.04$ and 0.16 due to the coexistence of SDW and superconductivity [13,20]. The asymmetry of the coherence peaks was also observed by the STM experiments [23-25].

In summary, we have studied the electronic and magnetic properties in the electron underdoped iron pnictides. Due to strong electron correlations, the domain walls are formed at the twin boundaries producing below the structural transition of the parent compounds. The existence of the domain wall structures leads to the nonuniformity of the electron density and the superconducting order parameter in real space. Therefore, inhomogeneity of superconductivity is intrinsic in the underdoped iron pnictides. The 90° domain walls and the supercurrent properties on them have been confirmed by the STM and SQIDM experiments. However, the anti-phase domain walls at the higher electron doping are not experimentally reported yet. We hope that such a magnetic structure could be verified by future STM experiments.

The authors would like to thank S. H. Pan, Ang Li and Yi Gao for useful discussions. This work was supported by the Texas Center for Superconductivity at the University of Houston and by the Robert A. Welch Foundation under Grant No. E-1146. Huang also acknowledge the support of Shanghai Leading Academic Discipline Project (project number S30105) and Shanghai Education Development Project.

- [1] Y. Kamihara, T. Watanabe, M. Hirano and H. Hosono, J. Am. Chem. Soc. **130**, 3296 (2008).
- [2] Zhi-An Ren, Wei Lu, Jie Yang, Wei Yi, Xiao-Li Shen, Zheng-Cai Li, Guang-Can Che, Xiao-Li Dong, Li-Ling Sun, Fang Zhou, and Zhong-Xian Zhao, Chin. Phys. Lett. **25**, 2215 (2008).
- [3] X. H. Chen, T. Wu, G. Wu, R. H. Liu, H. Chen, and D. F. Fang, Nature (London) **453**, 761 (2008).
- [4] C. de la Cruz, Q. Huang, J. W. Lynn, Jiying Li, W. Ratcliff II, J. L. Zarestky, H. A. Mook, G. F. Chen, J. L. Luo, N. L. Wang, and Pengcheng Dai, Nature (London) **453**, 899 (2008).
- [5] G. F. Chen, Z. Li, D. Wu, G. Li, W. Z. Hu, J. Dong, P. Zheng, J. L. Luo, and N. L. Wang, Phys. Rev. Lett. **100**, 247002 (2008).
- [6] Y. Laplace, J. Bobroff, F. Rullier-Albenque, D. Colson, and A. Forget, Phys. Rev. B **80**, 140501 (2009).
- [7] M.-H. Julien, H. Mayaffre, M. Horvatic, C. Berthier, X. D. Zhang, W. Wu, G.F. Chen, N.L. Wang, and J.L. Luo, Europhys. Lett. **87**, 37001 (2009).
- [8] I. I. Mazin and M. D. Johannes, Nature Phys. **5**, 141 (2009).
- [9] Lev P. Gor'kov and Gregory B. Teitel'baum, arXiv:1001.4641.
- [10] T.-M. Chuang, M. P. Allan, Jinho Lee, Yang Xie, Ni Ni, S. L. Budko, G. S. Boebinger, P. C. Canfield, and J. C. Davis, Science **327**, 181 (2010).
- [11] B. Kalisky, J. R. Kirtley, J. G. Analytis, J.-H. Chu, A. Vailionis, I. R. Fisher, and K. A. Moler, Phys. Rev. B **81**, 184513 (2010).
- [12] Guorong Li, Xiaobo He, Ang Li, Shuheng H. Pan, Jiandi Zhang, Rongying Jin, A. S. Sefat, M. A. McGuire, D. G. Mandrus, B. C. Sales, and E. W. Plummer, arXiv:1006.5907.
- [13] Degang Zhang, Phys. Rev. Lett. **103**, 186402 (2009); *ibid*, **104**, 089702 (2010).
- [14] H. Ding, P. Richard, K. Nakayama, T. Sugawara, T. Arakane, Y. Sekiba, A. Takayama, S. Souma, T. Sato, T. Takahashi, Z. Wang, X. Dai, Z. Fang, G. F. Chen, J. L. Luo, and N. L. Wang, Europhys. Lett. **83**, 47001 (2008).
- [15] D. H. Lu, M. Yi, S.-K. Mo, A. S. Erickson, J. Analytis, J.-H. Chu, D. J. Singh, Z. Hussain, T. H. Geballe, I. R. Fisher, and Z.-X. Shen, Nature (London) **455**, 81 (2008).
- [16] C. Liu, G. D. Samolyuk, Y. Lee, N. Ni, T. Kondo, A. F. Santander-Syro, S. L. Bud'ko, J. L. McChesney, E. Rotenberg, T. Valla, A. V. Fedorov, P. C. Canfield, B. N. Harmon, and A. Kaminski, Phys. Rev. Lett. **101**, 177005 (2008).
- [17] T. Kondo, A. F. Santander-Syro, O. Copie, Chang Liu, M. E. Tillman, E. D. Mun, J. Schmalian, S. L. Bud'ko, M. A. Tanatar, P. C. Canfield, and A. Kaminski, Phys. Rev. Lett. **101**, 147003 (2008).
- [18] V. B. Zabolotnyy, D. S. Inosov, D. V. Evtushinsky, A. Koitzsch, A. A. Kordyuk, G. L. Sun, J. T. Park, D. Haug, V. Hinkov, A. V. Boris, C. T. Lin, M. Knupfer, A. N. Yaresko, B. Buechner, A. Varykhalov, R. Follath, and S. V. Borisenko, Nature (London) **457**, 569 (2009).
- [19] K. Terashima, Y. Sekiba, J. H. Bowen, K. Nakayama, T. Kawahara, T. Sato, P. Richard, Y.-M. Xu, L. J. Li, G. H. Cao, Z.-A. Xu, H. Ding, and T. Takahashi, PNAS **106**,

- 7330 (2009) .
- [20] Tao Zhou, Degang Zhang, and C. S. Ting, Phys. Rev. B **81**, 052506 (2010).
 - [21] Yi Gao, Tao Zhou, C. S. Ting, and Wu-Pei Su, arXiv:1003.2609.
 - [22] Yi Gao *et al.*, in preparation.
 - [23] Y. Yin, M. Zech, T. L. Williams, X. F. Wang, G. Wu, X. H. Chen, and J. E. Hoffman, Phys. Rev. Lett. **102**, 097002 (2009).
 - [24] F. Massee, Y. Huang, R. Huisman, S. de Jong, J.B. Goedkoop, and M.S. Golden, Phys. Rev. B **79**, 220517(R) (2009).
 - [25] Ang Li *et al.*, (to be published).
 - [26] Lei Shan, Yong-Lei Wang, Bing Shen, Bin Zeng, Yan Huang, Ang Li, Da Wang, Huan Yang, Cong Ren, Qiang-Hua Wang, Shuheng Pan, and Hai-Hu Wen , arXiv:1005.4038.
 - [27] M. D. Lumsden, A. D. Christianson, D. Parshall, M. B. Stone, S. E. Nagler, G.J. MacDougall, H. A. Mook, K. Lokshin, T. Egami, D. L. Abernathy, E. A. Goremychkin, R. Osborn, M. A. McGuire, A. S. Sefat, R. Jin, B. C. Sales, and D. Mandrus, Phys. Rev. Lett. **102**, 107005 (2009).
 - [28] D. K. Pratt, W. Tian, A. Kreyssig, J. L. Zarestky, S. Nandi, N. Ni, S. L. Budko, P. C. Canfield, A. I. Goldman, and R. J. McQueeney , Phys. Rev. Lett. **103**, 087001 (2009).
 - [29] A. D. Christianson, M. D. Lumsden, S. E. Nagler, G. J. MacDougall, M. A. McGuire, A. S. Sefat, R. Jin, B. C. Sales, and D. Mandrus, Phys. Rev. Lett. **103**, 087002 (2009).
 - [30] D. S. Inosov, J. T. Park, P. Bourges, D. L. Sun, Y. Sidis, A. Schneidewind, K. Hradil, D. Haug, C. T. Lin, B. Keimer, and V. Hinkov, Nature Phys. **6**, 178 (2010).